Comparison of solid phase closure models in Eulerian-Eulerian simulations of a circulating fluidized bed riser

Nikku Markku, Daikeler Alexander, Stroh Alexander, Myöhänen Kari

DOI: 10.1016/j.ces.2018.11.031

COMPARISON OF SOLID PHASE CLOSURE MODELS IN EULERIAN-EULERIAN SIMULATIONS OF A CIRCULATING FLUIDIZED BED RISER

Markku Nikku[1*], Alexander Daikeler[2], Alexander Stroh[2], Kari Myöhänen[1]

[1]*Lappeenranta University of Technology, LUT Energy, PL 20, FI-53851 Lappeenranta, Finland*

[2]*Institute for Energy Systems and Technology, Technische Universität Darmstadt, Otto-Berndt Straße 2, D-64287 Darmstadt, Germany*

**Corresponding author email: mnikku@lut.fi*

ABSTRACT

In this work, computational fluid dynamics with Eulerian-Eulerian modeling approach is used in the investigation of the effect of the solid phase closure models on the hydrodynamics of a circulating fluidized bed riser. The studied models are the kinetic theory of granular flow and the powder modulus model. Computational performance and model prediction accuracy are investigated by performing transient simulations for three different cases and for different mesh sizes. The modeling results are compared with measured vertical pressure profile, external circulation mass flow rates, and particle velocity and concentration profiles obtained from a laboratory scale circulating fluidized bed unit. Additionally the computational times are compared to estimate the computational performance and to investigate if a simpler set of closures is computationally more affordable. The results indicate that both closure models can give good predictions for some quantities, while lacking in other quantities. The results indicate that the closure models for the solid phase have a noticeable effect on the model predictions, such as the vertical pressure profile and external circulation rate of the particles.

1. Introduction

Numerical modeling is a widely used tool in investigation of new designs and concepts, and for gaining detailed insight on the studied process. Especially with applications such as fluidized beds, where comprehensive measurements are not feasible, modeling can illustrate and help to understand the strong coupling that exists between the multiphase flow, chemical reactions and heat transfer on different time and length scales. However, there are many models available for describing the occurring physical phenomena and several different combinations can be made. To estimate which model combinations work and to verify the representativeness of the modeling results, measurement data is required for comparison.

Often time averaged pressure measurements from the fluidized bed riser are used to estimate the vertical particle distribution within the riser. However, this offers only very limited information about the distribution of particles and no information about their movement. The local particle concentrations and velocities have been measured by inserting different types of probes in to the riser, for example optical (Dubrawski et al., 2013; Johnsson and Johnsson, 2001; Magnusson et al., 2005; Pugsley et al., 2003; Ye et al., 2009) and capacitance based (Ellis et al., 2004; Malcus et al., 2000; Weber et al., 2018; Wiesendorf and Werther, 2000; Yang et al., 2018). Also non-intrusive methods based on tomography (Chan et al., 2009; Chaouki et al., 1997; de Velden et al., 2008; Maurer et al., 2015; Tortora et al., 2008) have been used.

There are many different approaches in modeling fluidized beds that differ in the level of detail and applicability. The most detailed methods solve the movement of the individual particles and are limited to small scale applications, namely the discrete element method (Jalali et al., 2013; Lu et al., 2015), while less detailed methods, such as Eulerian-Eulerian (Nikku et al., 2016; Shah et al., 2015a) or Eulerian-Lagrangian approach with particle grouping methods (Adamczyk et al., 2014a, 2014b; Nikolopoulos et al., 2017), are able to simulate even large industrial applications. In an ideal case, where computational power would be abundant, methods such as direct numerical simulation (DNS) and discrete element method (DEM) would be used to solve the different flow related quantities with minimal amount of numerical modeling involved in the simulations. However, as these methods are still very computationally expensive and limited to small system, less detailed solution methods with various approximating models have to be utilized when simulating the behavior of the fluid-particle system, and the simulation becomes sensitive on the selected models and the closures. Currently the kinetic theory of granular flow (KTGF) (Lun et al., 1984; Lun and Savage, 1986) is widely used to provide the closures for the solid phase in Eulerian-Eulerian modeling of fluidized beds. The closures in question are related to the different stresses, viscosity terms and solids pressure, with detailed discussion and possible submodels presented by van Wachen et al. (2001) and Qiu et al. (2017).

In bubbling fluidized beds, where the collision frequency between the particles is high, the effects of solid closures have been studied for example by Passalacqua et al. (2009) and Farzaneh et al. (2015) who examined the effect of frictional stress models. Zhao et al. (2015) investigated the influence of collisional parameters, and Patil et al. (2005a) studied the effects of the solid phase viscosity models. On circulating fluidized beds, the drag force between the gas and solid phases is widely considered to dominate the fluidization process. This has led to the research focusing on the effect of the momentum exchange modeling (Armstrong et al., 2010; Bona et al., 2013; Cloete et al., 2011; Shah et al., 2016, 2015b; Zhou et al., 2013), while limited number of works focusing on the solid phase stress closures could be found (Alves and Mori, 1998; Qiu et al., 2017; van Wachem et al., 2001). Other often studied parameters include the friction between the particles and walls (Armstrong et al., 2010; Cloete et al., 2011; Jin et al., 2010; Shah et al., 2016; Zhao et al., 2016; Zhou et al., 2013), friction between the particles (Cloete et al., 2011; Jin et al., 2010; Zhou et al., 2013), and the gas phase turbulence models (Cloete et al., 2011; Shah et al., 2016; Zheng et al., 2001).

In this work, the Eulerian-Eulerian approach is used in the investigation of the effect of closure model sets for the solid phase on the circulating fluidized bed (CFB) riser hydrodynamics. The studied model set are the kinetic theory of granular flow (KTGF) and the powder modulus (PM) model. The hypothesis is that using a simplified closure model set increases the computational performance, as the more sophisticated and physical KTGF is more computationally demanding due to increased number of parameters and equations to solve. Another hypothesis is that the accuracy of the KTGF model set simulations is better than the PM model set simulations. These hypotheses are tested by performing transient Eulerian-Eulerian simulations for three different cases, and with different mesh sizes for one case, using both of the above mentioned closures for the solid phase. The modeling results are compared with measurement data from a laboratory scale CFB unit to estimate the accuracy. Additionally, the computational times are compared to estimate the computational performance.

2. Experimental methods

Measurements were conducted in a laboratory scale CFB device. A schematic representation of the device is presented in Figure 1. The riser has a diameter of 0.213 m and height of 3.078 m with several pressure measurement connections placed along the height of the riser. The riser is operated with air blown through a fan and a measuring orifice is used to set the air flow. Fluidization gas for the loop seal is provided by an air compressor. There are additional measurement ports for capacitance probe measurements.

The solids loading of the riser was maintained at a constant level of 9 kg of sand, which has the material density of 2647 kg/m³. The density of the fluidization air at the inlet conditions was approximately 1.2 kg/m³ and the viscosity $2.0 \cdot 10^{-5}$ Pa s. The particle size distribution of the sand was determined by sieving, with the Sauter mean diameter of 193 µm. The sand particles have a roughly spherical shape, which allows the simplification to perfect spheres. The device was operated in a circulating fluidized bed mode in three different cases. Case A, B and C had fluidization velocities of 2.7, 2.3 and 1.9 m/s, respectively. Gas flow rate to the loopseal was kept constant at 6 m_n^3/h. Total of 22 differential pressure transducers were used to measure the vertical pressure profile in the riser. The mass flow rate of the particles to the cyclone was estimated by briefly stopping fluidization in the loopseal and measuring the particle accumulation to a defined control volume, holding approximately 400 grams. After filling the control volume, the fluidization of the loop seal was continued for several minutes before the test was repeated. The minimum number of mass flow rate measurements was 10 repetitions before averaging.

Capacitance probes were used in the measurement of volume concentrations and vertical velocities of the solids. The electrical capacitance of the gas - solids flow is measured within the sensing volume of approximate cylindrical dimensions of 10 mm in length and 8 mm in diameter. Solids concentrations are derived from the measured electrical capacitance by using an empirically derived relationship (Wiesendorf and Werther, 2000). Solids velocities are determined by cross correlating the signals of two vertically aligned probes with a center to center distance of 12 mm. Results are averaged over a measurement time of 64 seconds, which equals 500,000 recorded values at a measurement frequency of 7812 Hz. More detailed information on the capacitance probe measurements can be found from Daikeler et al. (2017). The probe measurement ports are illustrated in Figure 1. All measurement levels have two probe measurement ports named L and R, which are directly opposite each other. For some levels an additional M port was used, which has a 90° angle to the L and R ports. For case C, the used probe measurement ports are located as follows: L port at 124, 248 and 372 mm from the grid; L, M and R ports at 496, 992 and 1580 mm; and L and R ports at 2262 mm. For cases A and B, fewer measurement ports were used: for case A 248, 496, 992, 1580 and 2262 mm L ports and 496 and 992 mm M ports; while case B had only 496, 992, 1580 and 2262 mm L ports and R port at 2262 mm from the grid.

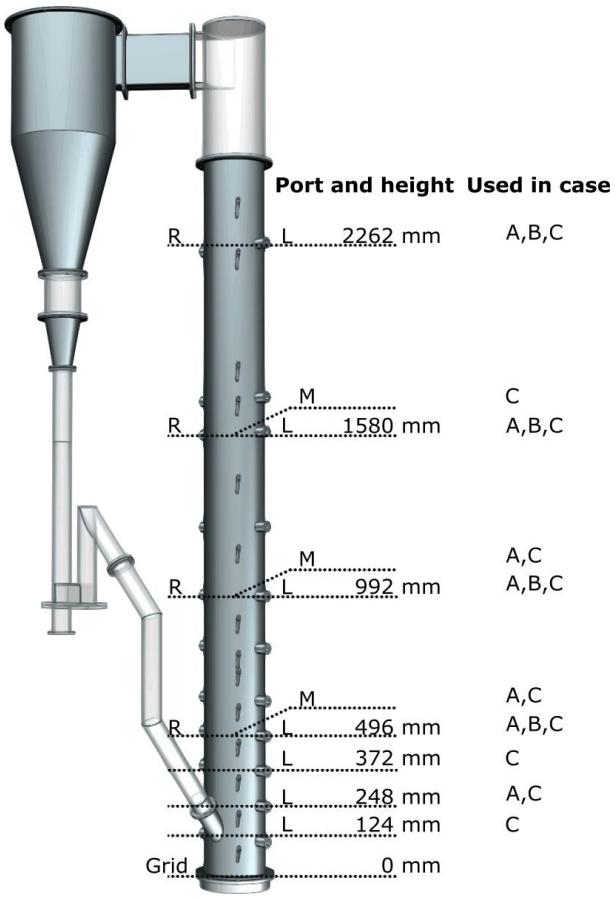

Figure 1. The schematic of the laboratory scale CFB device, showing the inclined pressure tabs and capacitance probe measurement ports.

3. Numerical methods

3.1. Eulerian-Eulerian model

Eulerian-Eulerian (also called as two-fluid) approach was used in simulation of the CFB device. In this approach, both the continuous phase (the fluid) and the discrete phase (the solid particles) are described as fluid and appropriate models have to be used to present the fluid-like properties of the solids. Equations 1 and 2 present the continuity equations, and Equations 3 and 4 present the momentum conservation equations for the gas and the solid phase, respectively. In this work, no phase change occurs, and no additional forces or source term are considered, thus the source terms on the following equations are zero.

$$\frac{d}{dt}\left(\alpha_{\mathrm{g}}\rho_{\mathrm{g}}\right)+\nabla\cdot\left(\alpha_{\mathrm{g}}\rho_{\mathrm{g}}\mathbf{u}_{\mathrm{g}}\right)=\sum S_{\mathrm{g}} \tag{1}$$

$$\frac{d}{dt}\left(\alpha_{\mathrm{s}}\rho_{\mathrm{s}}\right)+\nabla\cdot\left(\alpha_{\mathrm{s}}\rho_{\mathrm{s}}\mathbf{u}_{\mathrm{s}}\right)=\sum S_{\mathrm{s}} \tag{2}$$

$$\frac{d}{dt}\left(\alpha_{\mathrm{g}}\rho_{\mathrm{g}}\mathbf{u}_{\mathrm{g}}\right)+\nabla\cdot\left(\alpha_{\mathrm{g}}\rho_{\mathrm{g}}\mathbf{u}_{\mathrm{g}}\mathbf{u}_{\mathrm{g}}\right)=-\alpha_{\mathrm{g}}\nabla p+\nabla\cdot\bar{\tau}_{\mathrm{g}}+\alpha_{\mathrm{g}}\rho_{\mathrm{g}}\mathbf{g}-K_{\mathrm{gs}}\left(\mathbf{u}_{\mathrm{g}}-\mathbf{u}_{\mathrm{s}}\right)+\sum F_{\mathrm{g}}+\sum S_{\mathrm{g}} \tag{3}$$

$$\frac{d}{dt}\left(\alpha_{\mathrm{s}}\rho_{\mathrm{s}}\mathbf{u}_{\mathrm{s}}\right)+\nabla\cdot\left(\alpha_{\mathrm{s}}\rho_{\mathrm{s}}\mathbf{u}_{\mathrm{s}}\mathbf{u}_{\mathrm{s}}\right)=-\alpha_{\mathrm{s}}\nabla p-\nabla p_{\mathrm{s}}+\nabla\cdot\bar{\tau}_{\mathrm{s}}+\alpha_{\mathrm{s}}\rho_{\mathrm{s}}\mathbf{g}+K_{\mathrm{gs}}\left(\mathbf{u}_{\mathrm{g}}-\mathbf{u}_{\mathrm{s}}\right)+\sum F_{\mathrm{s}}+\sum S_{\mathrm{s}} \tag{4}$$

Simulations were performed with OpenFOAM 5.0 with the solver *reactingTwoPhaseFoam*. The solver can utilize the kinetic theory of granular flows (KTGF) (Gidaspow et al., 1991) approach for Eulerian-Eulerian two-phase modeling as well as a so-called powder modulus (PM) approach, discussed later. The closures investigated in this work are related to the solids pressure p_s and shear stress τ_s terms in Equation 4. The closures related to the kinetic theory of granular flow are presented in Table 1, while the powder modulus closures are presented in Table 2. The drag model presented by Gidaspow et al. (1991) utilizes Equations 5 and 6 (Wen and Yu, 1966) for dilute suspensions and Equation 7 (Ergun, 1952) for dense suspension.

$$K_{gs} = \frac{3}{4} C_D \frac{\alpha_s \alpha_g \rho_g \left| \mathbf{u}_g - \mathbf{u}_s \right|}{d_s} \alpha_g^{-2.65} \quad \alpha_g > 0.8 \tag{5}$$

$$C_D = \begin{cases} \frac{24}{\mathrm{Re}} \left(1 + 0.15\,\mathrm{Re}^{0.687}\right) & \mathrm{Re} \le 1000 \\ 0.44 & \mathrm{Re} > 1000 \end{cases} \tag{6}$$

$$K_{gs} = 150 \frac{\alpha_s \left(1 - \alpha_g\right) \mu_g}{\alpha_g d_s^2} + 1.75 \frac{\rho_g \alpha_s \left| \mathbf{u}_g - \mathbf{u}_s \right|}{d_s} \quad \alpha_g \le 0.8 \tag{7}$$

Enwald et al. (1996) present two different options for solids pressure formulations, the kinetic theory of granular flow and what the authors called an “alternative traditional approach”, which is based on experiments. Massoudi et al. (1992) referred to this alternative approach as a modulus, Qiu et al. (2017) and Patil et al. (2005a, 2005b) refer to a constant viscosity model with a modulus of elasticity, and Peltola (2009) used a term powder modulus or particle normal force model. In this work the term powder modulus (PM) will be used. Several of different powder modulus models have been listed by Enwald et al. (1996) and Massoudi et al. (1992), and they are compared in Figure 2. Some of the models are clearly limited to affect only in very dense suspensions with minimal effect on dilute systems, while others have significantly larger effect also in more dilute suspensions. Another interesting feature is that there is a lot of variation in the powder modulus values between different models, even several orders of magnitude for the same volume fraction. The function of the powder modulus is to prevent over packing of the solids, which would lead to unphysical results and might cause instability. It can be noted that the model used in this work is very close to the model presented by Syamlal and O´Brien.

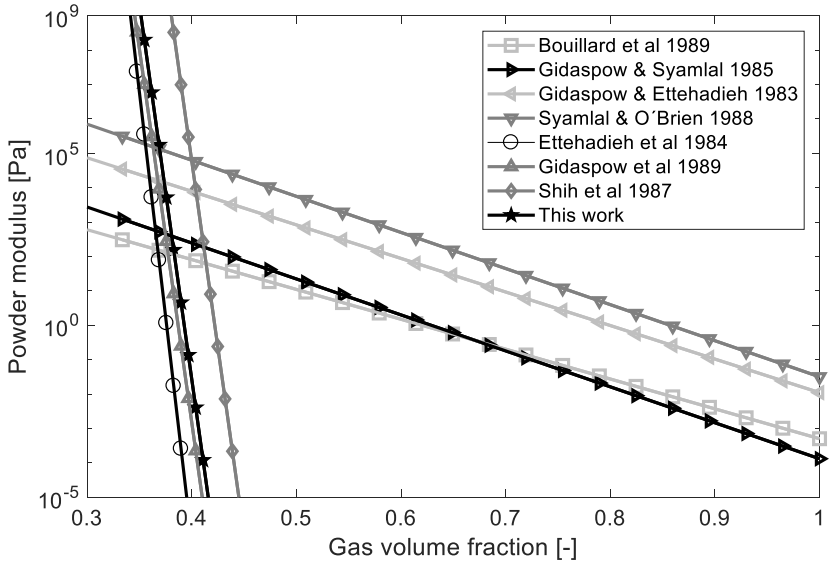

Figure 2. Comparison of various powder modulus models, after Enwald et al. (1996) and Massoudi et al. (1992).

Table 1. The models used for the kinetic theory of granular flow simulations.

Phase stress-strain tensors

$$\tau_g = \alpha_g \mu_g \left(\nabla \mathbf{u}_g + \nabla \mathbf{u}_g^T\right) - \frac{2}{3}\alpha_g \mu_g \left(\nabla \cdot \mathbf{u}_g\right) I$$

$$\tau_s = \alpha_s \mu_s \left(\nabla \mathbf{u}_s + \nabla \mathbf{u}_s^T\right) + \alpha_s \left(\lambda_s - \frac{2}{3}\mu_s\right)\left(\nabla \cdot \mathbf{u}_s\right) I$$

Solid shear viscosity $\mu_s = \mu_{s,col} + \mu_{s,kin} + \mu_{s,fr}$ (Syamlal et al., 1993), (Schaeffer, 1987)

$$\mu_{s,col} = \frac{4}{5}\alpha_s \rho_s d_s g_{0,ss}\left(1+e_{ss}\right)\left(\frac{\Theta_s}{\pi}\right)^{0.5}$$

$$\mu_{s,kin} = \frac{\alpha_s \rho_s d_s \sqrt{\Theta_s \pi}}{6\left(3-e_{ss}\right)}\left[1+\frac{2}{5}\left(1+e_{ss}\right)\left(3-e_{ss}-1\right)\alpha_s g_{0,ss}\right]$$

$$\mu_{s,fr} = \frac{\frac{1}{2}p_{fr}\sin\phi}{\sqrt{\frac{1}{3}I}}$$

Granular bulk viscosity (Lun et al., 1984)

$$\lambda_s = \frac{4}{3}\alpha_s \rho_s g_0 \left(1+e_s\right)\left(\frac{\Theta_s}{\pi}\right)^{0.5}$$

Solid pressure. (Lun et al., 1984)

$$p_s = \alpha_s \rho_s \Theta_s + 2\rho_s\left(1+e_{ss}\right)\alpha_s^2 g_{0,ss}\Theta_s$$

Frictional pressure (Johnson et al., 1990)

$$p_{fr} = \begin{cases} 0 & \alpha_s < \alpha_{s,f,min} \\ Fr\dfrac{\left(\alpha_s - \alpha_{s,f,min}\right)^n}{\left(\alpha_{s,max} - \alpha_s\right)^p} & \alpha_s \geq \alpha_{s,f,min} \end{cases}$$, where Fr=0.05, n=2 and p=5, $\alpha_{s,min}$=0.5.

Radial distribution function (Savage, 1988; Sinclair and Jackson, 1989)

$$g_{0,ss} = \left[1-\left(\frac{\alpha_s}{\alpha_{s,max}}\right)^{\frac{1}{3}}\right]^{-1}$$

Granular energy equation (Θ_s is the granular temperature)

$$\frac{3}{2}\left(\frac{d}{dt}\left(a_s \rho_s \Theta_s\right) + \nabla \cdot \left(a_s \rho_s \mathbf{v}_s \Theta_s\right)\right) = \left(-p_s \bar{\bar{I}} + \bar{\bar{\tau}}_s\right) : \nabla \mathbf{v}_s + \nabla \cdot \left(k_{\Theta s}\right)\nabla \Theta_s - \gamma_{\Theta s} + \phi_{ls}$$

Diffusion coefficient for granular energy (Syamlal et al., 1993)

$$k_{\Theta s} = \frac{15 d_s \rho_s \alpha_s \sqrt{\Theta_s \pi}}{4\left(41-33\eta\right)}\left[1+\frac{12}{5}\eta^2\left(4\eta-3\right)\alpha_s g_{0,ss} + \frac{16}{15\pi}\left(41-33\eta\right)\eta\alpha_s g_{0,ss}\right],$$

where $$\eta = \frac{1}{2}\left(1+e_{ss}\right)$$

Collisional dissipation of energy (Lun et al., 1984)

$$\gamma_{\Theta s} = \frac{12\left(1-e_{ss}^2\right)g_{0,ss}}{d_s\sqrt{\pi}}\alpha_s^2 \rho_s \Theta_s^{\frac{3}{2}}$$

Energy exchange between the gas and solid phase (Lun et al., 1984)

$$\phi_{gs} = -3K_{gs}\Theta_s$$

Table 2. The powder modulus model.

Phase stress-strain tensors $\tau_g = \alpha_g \mu_g \left(\nabla \mathbf{u}_g + \nabla \mathbf{u}_g^T\right) - \frac{2}{3} \alpha_g \mu_g \left(\nabla \cdot \mathbf{u}_g\right) I$ $\tau_s = 0$ Solid pressure – phasePressure model, described by Enwald et al. (1996) and Massoudi et al. (1992) $p_s = \alpha_s g_0 \exp\left(A\left(\alpha_s - \alpha_{s,max}\right)\right)$, where the coefficient constants are g_0=1000, A=500, and $\alpha_{s,max}$=0.62.

3.2. Simulation setup

The riser of the laboratory device was discretized to a structured computational mesh using Ansys ICEM CFD. For the mesh size, cell size of 10 times the particle size is given as a rule of thumb by Panday et al. (2014), which translates to approximately 2 mm for the average length of a cell side. This could not be used due to the large number of cells it would require. However, three different coarser mesh sizes were investigated for one case. The average lengths of cell sides are 10, 8 and 6 mm, which correspond to 50, 40 and 30 times the average particle diameter, respectively. The resulting mesh sizes are 176.000, 321.000 and 745.000 hexahedral elements, respectively. Figure 3 illustrates details from the used meshes. After comparison of the results with different mesh sizes, the 8 mm mesh was selected to be used for the simulations of two other cases as it offers more acceptable computational times with slightly higher resolution of the computational domain.

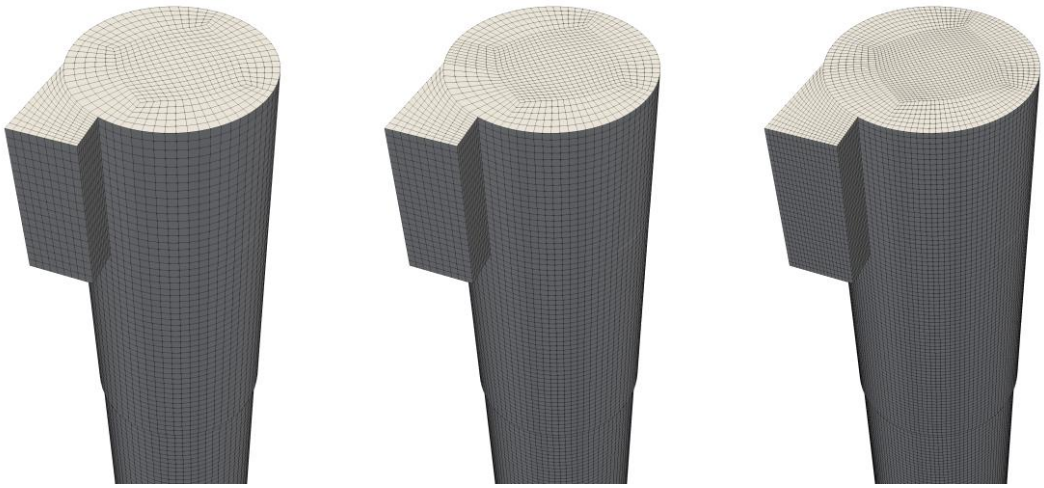

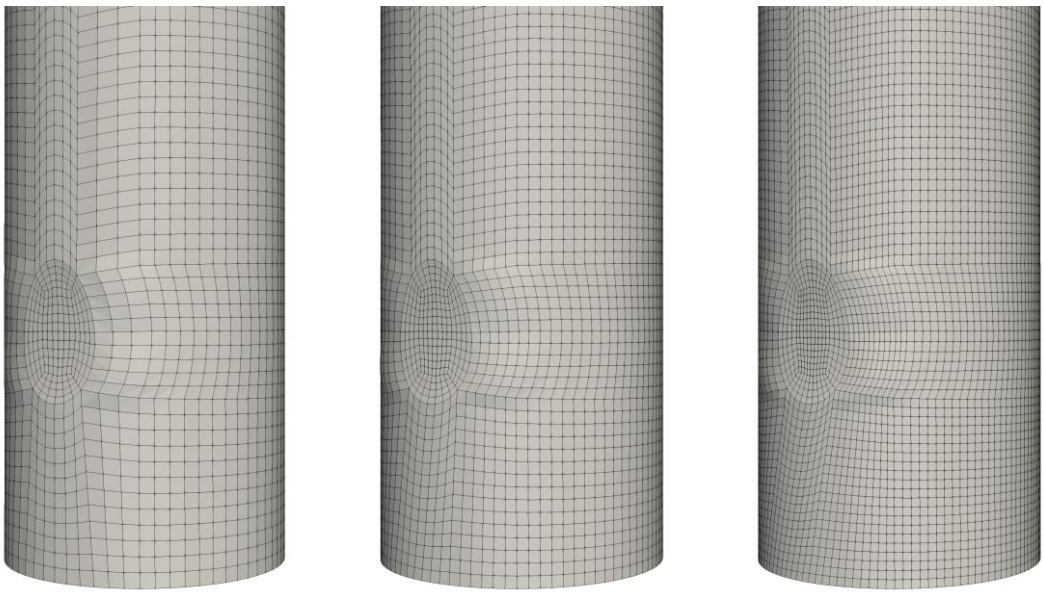

Figure 3. The computational meshes used. From left to right: 10 mm, 8 mm and 6 mm (average length of the cell side).

The objective of this work is to compare the simulation results with the two closure models. Two sets of model parameters, named KTGF for kinetic theory of granular flows and PM for powder modulus, are used with Table 3 presenting the utilized models for both model sets. The gas flow is simulated as laminar, similarly to Jalali et al (2018), and additionally no turbulence of the solid phase is considered in the used solver. The negligence of the solid phase turbulence in the KTGF model set is a common, but clear limitation in the taken modeling approach as demonstrated by Fox (2014). In this respect, both model sets are treated similarly, and this should have limited effect on the comparison of the closure models. The simulation results with the two closure models are compared with each other and with the measurement data, such the vertical pressure profile, external circulation rate of the solids and solids velocity and concentration profiles, to investigate their accuracy in predicting the riser hydrodynamics.

Table 3. List of the utilized models. Refer to Tables 1 and 2 for details. The model names and parameters are presented as they appear in the software.

	PM	**KTGF**
Drag	GidaspowErgunWenYu	GidaspowErgunWenYu
Lift	Not used	
Virtual mass	Not used	
Surface tension	Not used	
Gas flow model	Laminar	
Solids pressure	phasePressure	Lun
Granular temperature	-	Transport equation
Granular conductivity	-	Gidaspow
Granular viscosity	-	Gidaspow
Bulk viscosity	-	Lun et al
Radial distribution	-	SinclairJackson
Frictional stress	-	JohnsonJacksonSchaeffer
Frictional viscosity	-	Schaeffer
Angle of internal friction	-	28.5 *
Frictional pressure	-	JohnsonJackson
Frictional minimum packing limit	-	0.5 *
Solids packing limit	0.62	0.62

* Based on Johnson et al. (1990).

The initial values and boundary conditions of the simulations were set according to the values of the experiments. The system is considered as adiabatic with constant temperature set for the both phases for the whole domain, and material properties taken as they are described in section 2. The boundary conditions are presented in Table 4 for all cases. The granular temperature θ is only solved for the kinetic theory of granular flow, not for the powder modulus model. For the recirculation of the particles exiting the riser, a closure was implemented to keep the mass of the system constant. A custom code was used to compute the particle mass flow rate at the outlet and implement the same particle mass flow rate to the solids return inlet boundary. The air volume fraction is computed as unity minus the particle volume fraction.

Table 4. The boundary conditions for the all simulations. The boundary condition and names of the models are presented as they appear on the software.

	Grid	Solids return	Outlet	Walls
α_s	zeroGradient	custom code	zeroGradient	zeroGradient
u_s	fixedValue uniform (0 0 0)	surfaceNormalFixedValue A, B, C: 0.1 m/s	zeroGradient	JohnsonJackson-ParticleSlip, specularity 0.01
u_g	interstitialInletVelocity A: 2.7 m/s B: 2.3 m/s C: 1.9 m/s	surfaceNormalFixedValue A, B, C: 0.17 m/s	pressureInlet-OutletVelocity	noSlip
p_{rgh}	fixedFluxPressure	fixedFluxPressure	prghPressure	fixedFluxPressure
θ	zeroGradient	uniform 1e-4 $m^2 s^{-2}$	zeroGradient	JohnsonJackson-ParticleTheta, specularity 0.01, restitution 0.9

All simulations were carried out on a single computer, equipped with 4 Intel Xeon E7-8890 processors with a total of 144 cores and 2048 GiB of random access memory. Total of 36 cores were used for a single simulation. Each simulation was performed as transient and after the initialization and development of quasi-steady multiphase flow, flow data was time-averaged for 30 seconds. Courant number controlled adaptive time stepping was used with the maximum allowed Courant number of 0.2 and maximum time step of $1e^{-4}$ s. All time steps converged to steady level of residuals.

4. Results and discussion

For case A, the simulation using the KTGF model set couldn't be completed. Even after significantly reducing the maximum allowed time step and Courant number settings, the simulation would lead to overpacking in dense regions or reversed flow at the outlet and eventual divergence. These dense regions appear near the riser walls at the bottom of the riser, and they are also present in cases B and C, but no convergence issues were experienced in these cases. For case A the higher inner and outer circulation rates probably lead to higher solids concentrations compared to cases B and C. The measured pressure profiles also indicate significantly larger presence of particles in the bottom of the riser with case A. As for PM model set, though also predicting dense regions, the model set was able to prevent overpacking and results of PM model set are presented for case A, as well as for cases B and C, where results of KTGF model set are also available.

4.1. Pressure profiles

Figure 4 presents a comparison of the measured vertical pressure profiles for all simulated cases with both models. The KTGF model set results seem to match well to the measurements in the bottom and the top of the riser, while having larger differences between 0.15 and 1.38 m. In general, the PM model has better correspondence with the measurements throughout the riser height, especially in case C where the majority of the predictions are between the standard deviation of the measurements presented by the error bars. Between 1.65 and 2.36 m, the PM model seems to underestimate the pressure, while KTGF offers good correspondence. With both models, refining the mesh leads towards better correspondence with the measurements. The 10 mm and 8 mm mesh results are quite similar, with 8 mm having slightly lower values in the bottom of the riser, while showing slightly higher values after approximately 0.3 m. Reason for this behavior is unclear, though it is likely due to differing distributions of cells between the meshes. The 6 mm mesh offers the lowest pressure values, but it doesn't lead to improved accuracy for either model set. The results of case C are better in line with the measurements compared to cases A and B, where there are larger differences between 0.1 and 1.38 m. Both model sets seem to manage to predict the total pressure drop correctly in all cases.

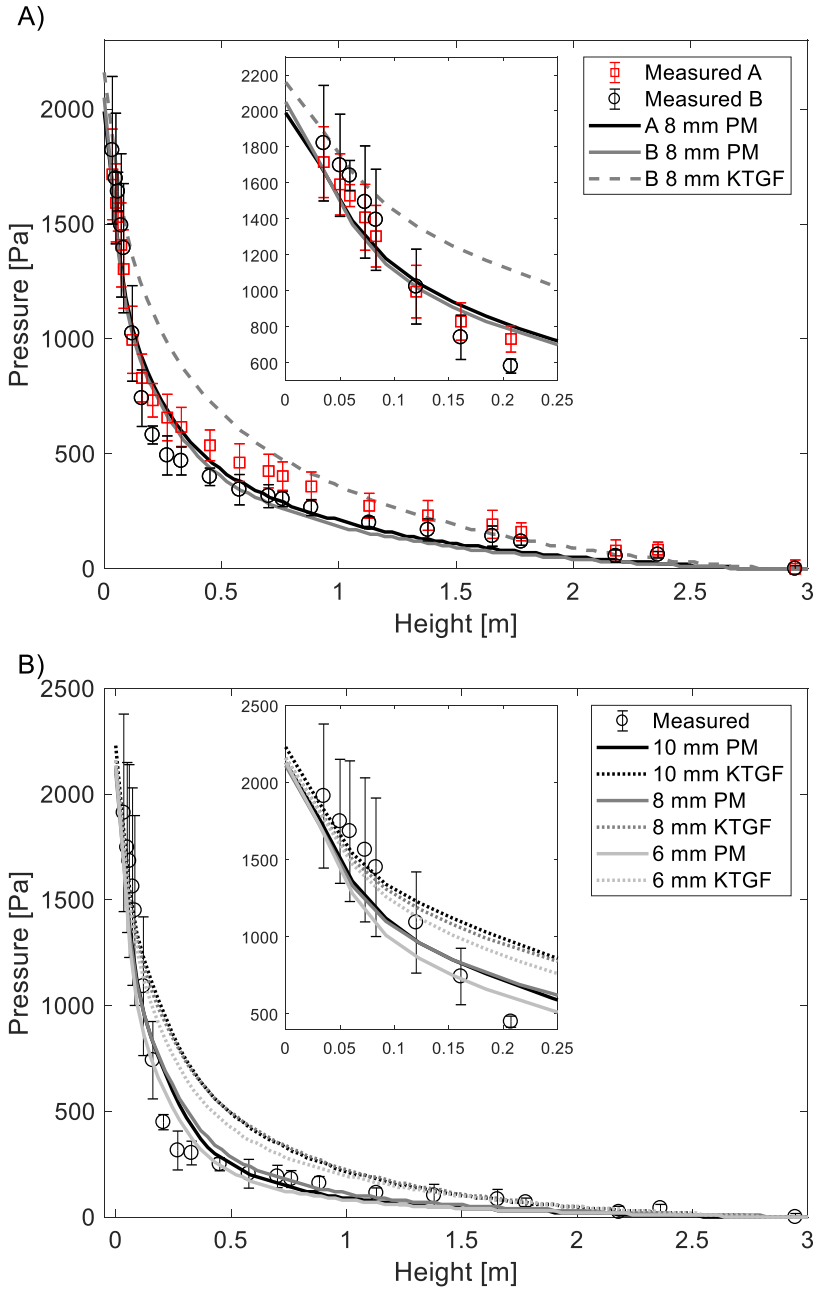

Figure 4. The comparison of vertical pressure profiles in the riser for A) cases A and B, and B) case C.

4.2. External circulation of particles

Table 5 presents the measured and modeled results of particle mass flow rates exiting the riser with standard deviation. For case C with all mesh sizes, the modeled results are significantly lower than the measured values, with the KTGF model set predicted average values being only 60 to 70 % and PM model set values 20 to 30 % of the averaged measured value. For PM model set, the circulation rates are 50 and 57 % of measured values in cases B and A, respectively. For the case B, KTGF model set predicts significantly higher mass flows, approximately 150 % of the measured value, which is closer to the values measured in case A.

Table 5. Measurements of external circulation rates of particles.

Case	Measured	KTGF 10 mm	PM 10 mm	KTGF 8 mm	PM 8 mm	KTGF 6 mm	PM 6 mm
A: 2.7 m/s	Mean: 334 g/s St. dev.: 20 g/s	-	-	-	192.0 51.4	-	-
B: 2.3 m/s	Mean: 220 g/s St. dev.: 11 g/s	-	-	345.5 88.9	109.9 27.3	-	-
C: 1.9 m/s	Mean: 101 g/s St. dev.: 4 g/s	67.9 19.7	25.4 6.9	77.8 19.0	30.9 9.1	65.0 15.2	22.7 5.9

4.3. Computational times

Calculations times for case C simulations with different meshes are presented in Table 6. For the coarsest mesh, the KTGF model set took only 88 % of the time required for the PM model set, while taking 91 % for the intermediate mesh and 103 % for the finest mesh used. This contradicts the hypothesis of a simplified model reducing the computational time. This contradiction is due to the adaptive time stepping used in the simulations, as the KTGF model set manages to use larger share of longer time steps compared to the PM model set. This situation is only reserved with the 6 mm mesh. For a fixed time step size, the PM model set is faster, with the KTGF model set computational times being 11, 9 and 6 % longer for the coarse, middle and fine mesh, respectively. This is in line with the original hypothesis, though using a fixed time step size is not beneficial due to increased computational times as previously demonstrated by Nikku et al. (2017).

Table 6. Computational times for case C simulations.

Case	KTGF 10 mm	PM 10 mm	KTGF 8 mm	PM 8 mm	KTGF 6 mm	PM 6 mm
C: 1.9 m/s	132 h	150 h	289 h	317 h	752 h	731 h

4.4. Comparison with the probe measurements on the probe location

The unweighted time averaged modeling results are compared with the probe measurements on the measurement path of the probe to give an exact comparison of local profiles for each measurement height. Depending on the measurement level, measurements could be carried out from left-to-right (noted as L), right-to-left (R) or from a port perpendicular to the previously mentioned (M). A mesh sensitivity study was performed first to study the effect of the mesh size using experimental case C as a reference due to extensive measurements.

For case C, the comparison of the modeled results with the probe measurements is presented in Figure 5 for the lower part and in Figure 6 for the upper part of the riser. For the lower part of the riser in

Figure 5, both models predict quite similar results with all meshes, with the PM model set using the 10 mm mesh standing out from the rest slightly. The solids volume fractions and axial velocities are predicted well with all cases in the bottom of the riser. There is a noticeable trend of increasing the overestimation of the volume fractions when moving higher in the riser. For the solids velocities, the PM cases predict slightly lower axial velocities than the KTGF, which better corresponds with the measured values.

In the upper part of the riser in Figure 6, the volume fraction predictions are separated more, with KTGF overestimating the volume fraction in all cases, while the PM cases offer good agreement, with the finest mesh offering the best correspondence. The agreement also improves as the height increases, with the two highest levels offering the best agreement in general. For the solids axial velocities, the KTGF cases offer the better agreement, whereas the PM cases underestimate axial velocities more. For the two highest measurement positions, the measurement profiles appear less symmetrical and there being larger difference between the measurement results taken from different directions (left to right vs right to left). This could be the effect of the outlet to cyclone, but unfortunately no higher measurement ports were available to confirm this hypothesis. The models predict more uniform profiles compared to the measurements, therefore failing to produce same peak level of velocities.

Overall, the effect of the mesh size is not clear. While the finest mesh produces the best correspondence with the measurements in some measurement locations, the differences to other meshes are not large. In the lower part of the riser, the differences between meshes are small with solids volume fraction, in the upper part, the finest mesh produces slightly lower values compared to very similar values of the other meshes. More variation is seen in the velocity profiles, where the fine and medium mesh both seem to give reasonably good results with KTGF compared with the measurements. In the upper part of the riser, also the coarsest mesh results of the KTGF are comparable with the finer mesh results and the measurements. The simulation results between the meshes were compared to determine mesh independence. The differences between the medium and the finest meshes for the pressure profile the differences were on average 8 % for the KTGF model set and 12 % for the PM model set. The differences in solids velocities averaged over different heights were 7 % with the KTGF model set and 11 % with the PM model set, and for the volume fraction 10 % with the KTGF model set and 16 % with the PM model set. Due to these small changes between the meshes, the other experimental cases A and B were only simulated with the medium sized mesh.

The modeled results of cases A and B are compared with the probe measurements in Figure 7. It can be noted that the probe measurement results have very similar shape between the cases, with the solids velocities at the core and solids concentrations near the walls being higher in case A than in case B. For case B the simulation results with KTGF and PM model sets are showing differences with the PM model set predicting lower solids concentrations and velocities for every height except 496 mm above the grid. The PM model set results are closer to the measured values of solids concentration while KTGF model set overpredicts the concentrations, as also visible as larger values in the pressure profile. Lower in the riser, the PM model set results are closer to the measured velocity values, while the KTGF model set offers better correspondence higher in the riser. The higher concentrations and velocities of the KTGF model set results are the cause of the higher external circulation rates, as more solids are elutriated higher in the riser and eventually to the riser exit. For case A, the PM model set overpredicts the concentrations and velocities in the lower part of the riser, while offering good agreement with the measurements higher in the riser, with very good correspondence in solids

velocity on level 992 and 1580 mm above the grid. In the upper part of the riser, the measured profiles show similar uneven distributions as with the case C, though with the case B the KTGF model set better matches the measured values, but still fails to predict the uneven distributions. Unfortunately, cases A and B have less measurements at the bottom of the riser compared to case C, thus limiting the comparison with the measurements in the region.

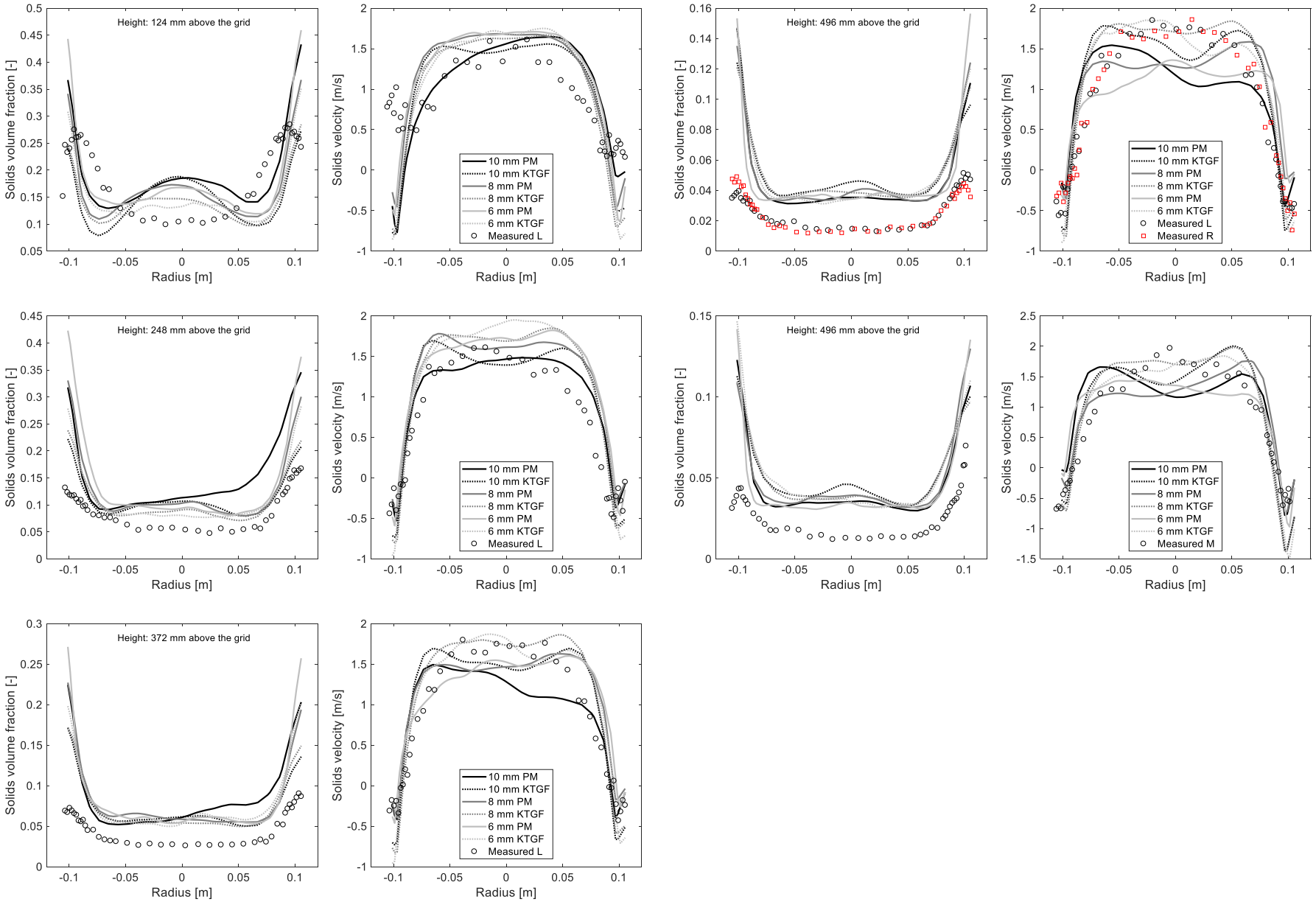

Figure 5. Direct comparison of the modeled results with the probe measurements in case C, the lower part of the riser.

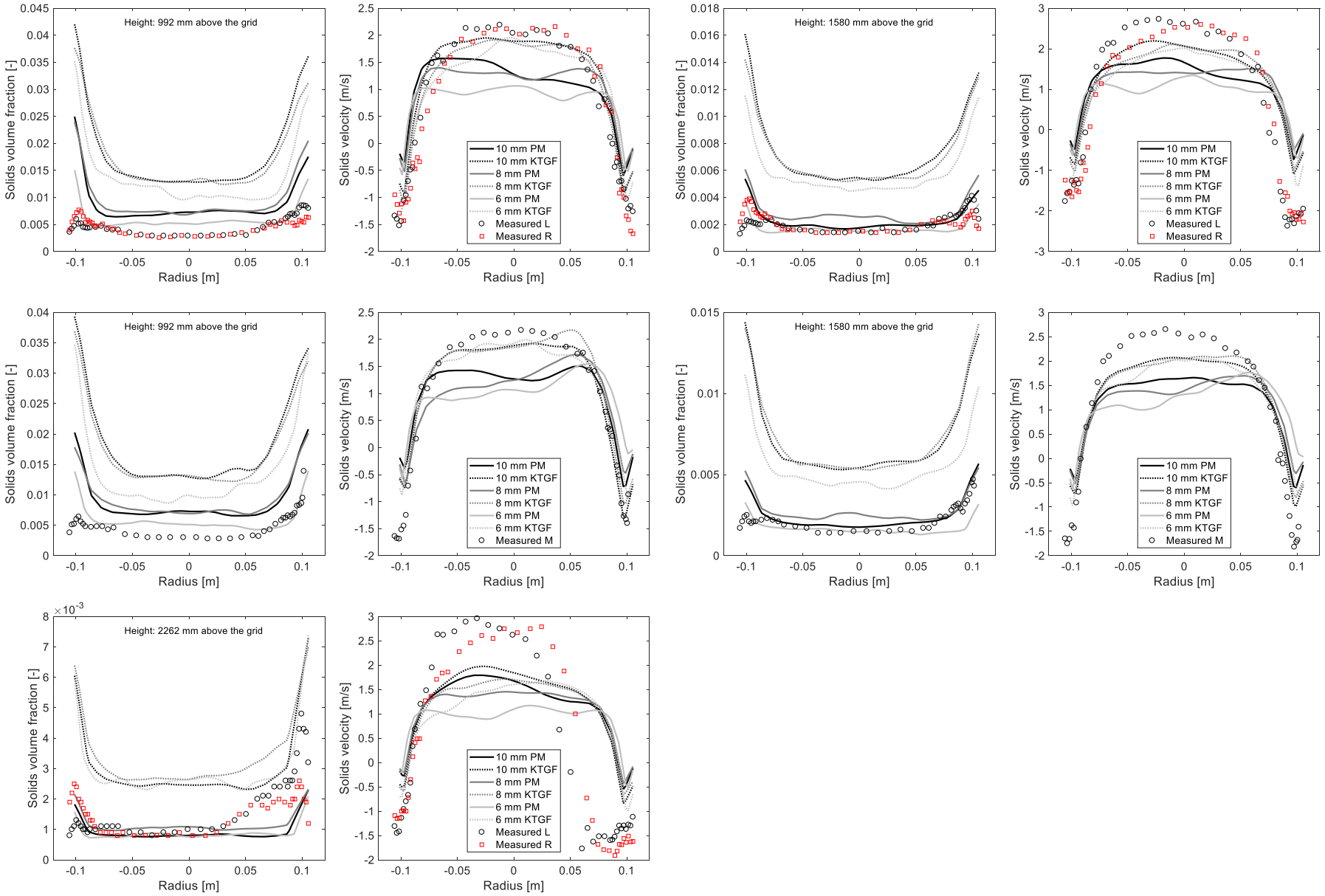

Figure 6. Direct comparison of the modeled results with the probe measurements in case C, the upper part of the riser.

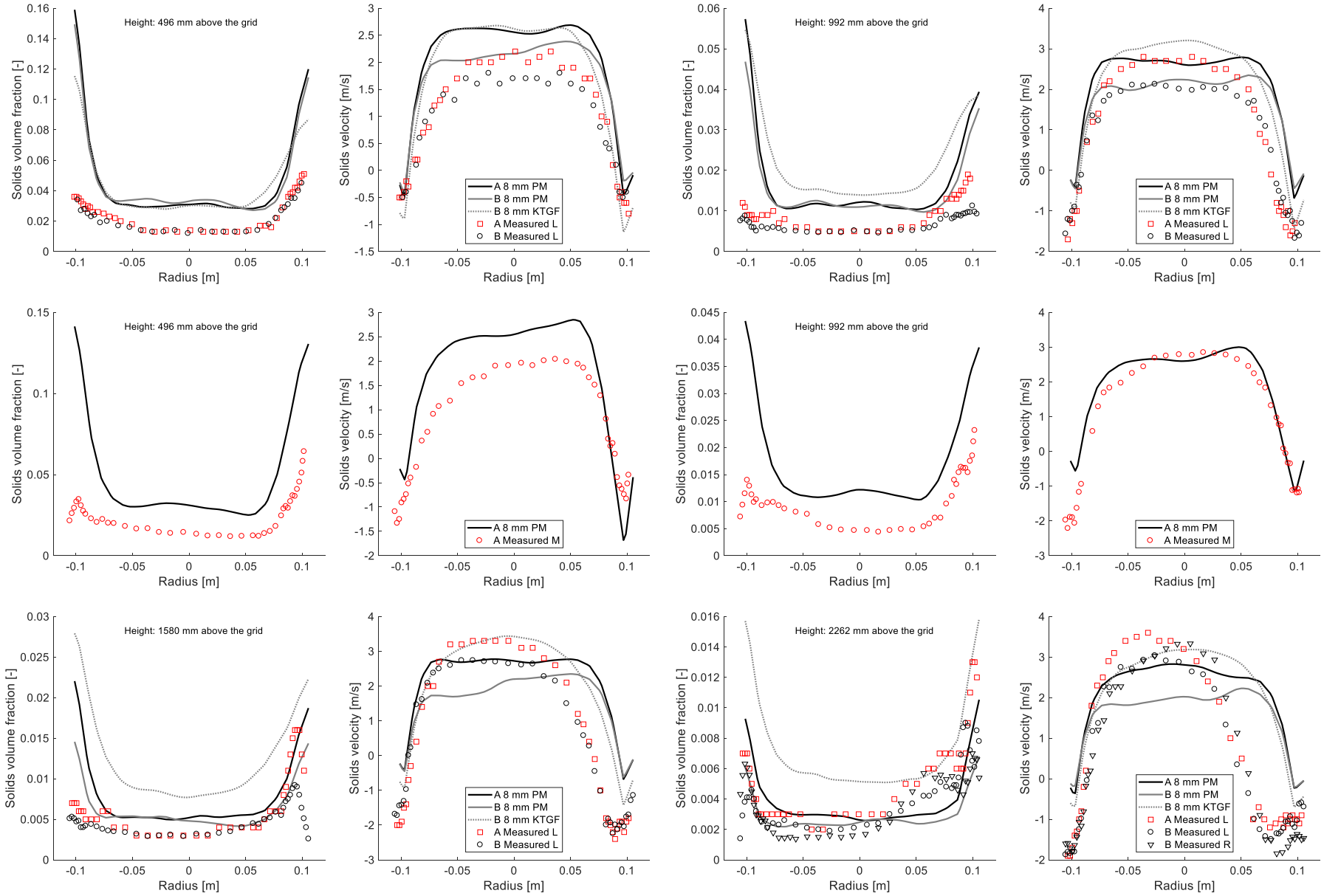

Figure 7. Direct comparison of the modeled results with the probe measurements in cases A and B.

4.5. Comparison with the probe measurements with cross-sectional average values

For each measurement height, the time averaged modeling results are averaged in radial direction for the cross sectional plane and compared with the probe measurements. Each plane is divided into 20 “rings” in radial direction, for which a single unweighted average value is produced to give a time and space averaged profile for each measurement height. In the following figures, the modeled results are mirrored for better comparison with the probe measurements.

For case C, the time and space averaged profiles are compared with the probe measurements in Figure 8. Comparing the time and space averaged profiles with only time averaged profiles from the probe measurement locations, it seems that there are only small differences. The space averaging results in flatter profiles in the core, but otherwise the profiles are quite similar to the local values. Given this, the measurements are also in quite good agreement with the time and space averaged modeling results. In the lower part of the riser, both models give very similar results with all meshes, with smaller differences in the axial velocities than with only the local values. In the upper part of the riser, similar agreement is seen, the PM corresponds better with the measured volume fractions while KTGF matches better with the measured axial velocities.

The time and space averaged profiles for cases A and B are presented in Figure 9. As with the case C, the probe measurements compare quite similarly to the time and space averaged profiles as they do with only the time averaged profiles from the measurement locations. There are significant disagreements in the lower part of the riser, while the results match better in the upper part. The PM model set profiles are more even at the core, while for case B the KTGF model set results tend to be more parabolic, both offer good estimation of the wall layer gradients in the upper part of the riser, with the PM model set agreeing somewhat better with the measured levels, except at the highest point. As already mentioned, the cases A and B didn’t have measurements in the lower part of the riser, but both model sets predict very similar behavior there in both cases.

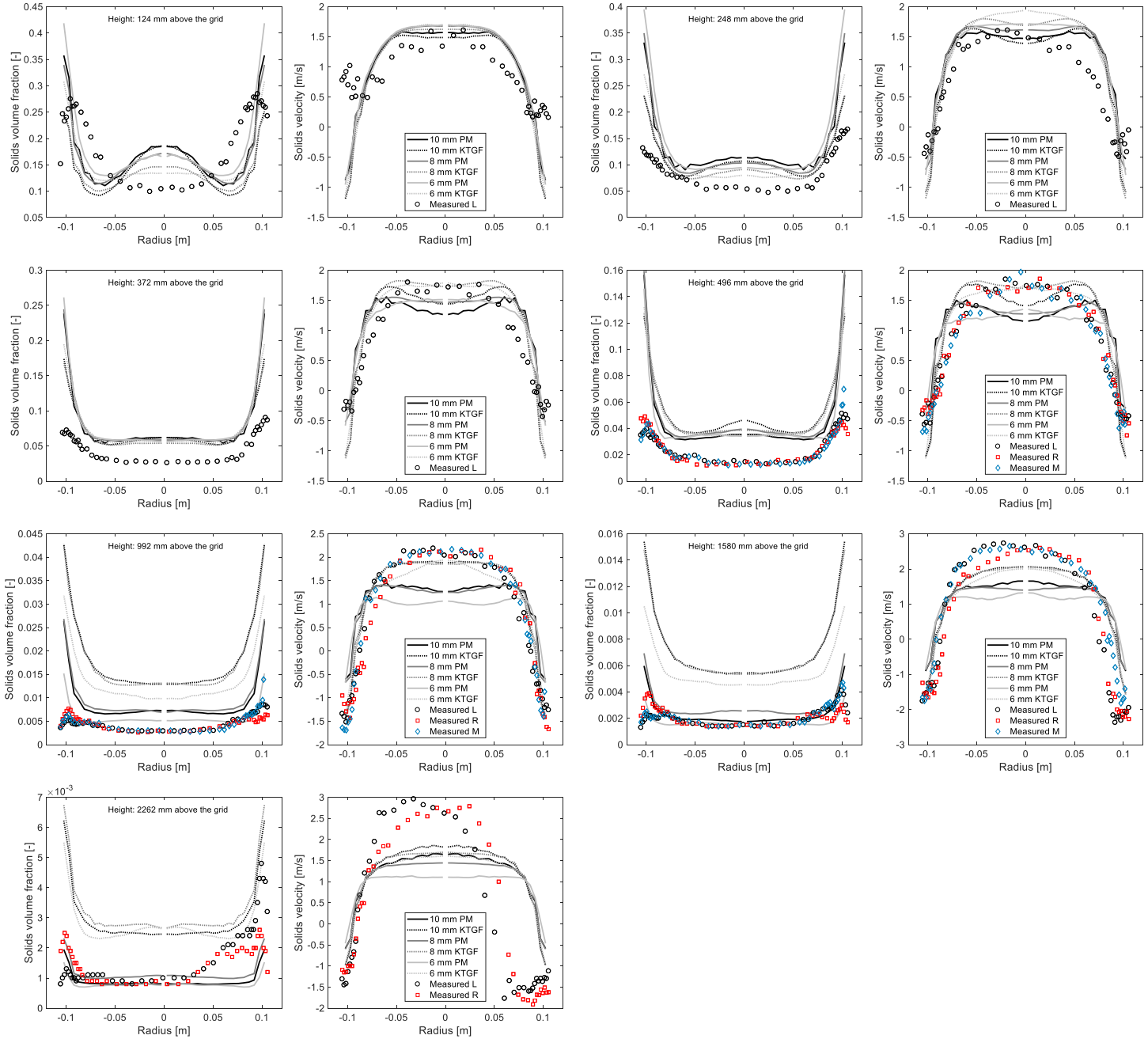

Figure 8. Time and space averaged profiles of gas velocity, solids velocities and solids volume fraction for case C.

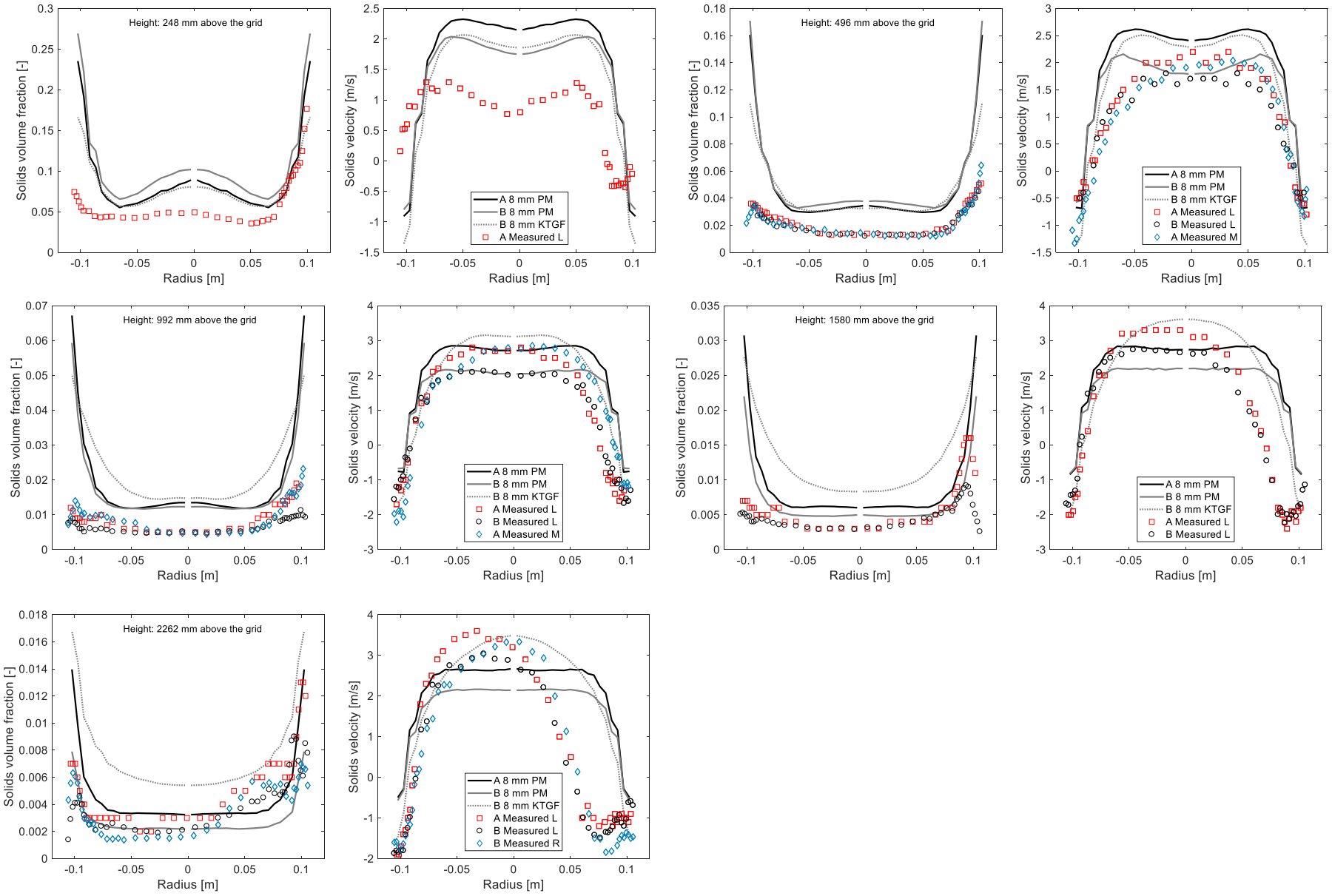

Figure 9. Time and space averaged profiles of gas velocity, solids velocities and solids volume fraction for cases A and B.

5. Conclusions

In this work, a laboratory scale CFB unit was modeled and the modeling results were compared with detailed measurements including solids profile data obtained with capacitance probe. The effect of solids closure models in Eulerian-Eulerian approach was investigated with powder modulus and kinetic theory of granular flow model sets.

The powder modulus model set was able to give good or better predictions than the kinetic theory of granular flow when compared with the experimental information, such as the vertical pressure profile and solids distribution, while not being able to accurately predict the solids velocities and circulation mass flow rates. Similar results were reported by Qiu et al. (2017). Kinetic theory of granular flow model set produced better estimates of the solids velocities and the circulation mass flow rates for the case with the lowest fluidization velocity (1.9 m/s) with slight underestimation, while overestimating the circulation rate significantly in a case with higher fluidization velocity (2.3 m/s). Based on the results, it cannot be stated that one model set would be better than the other in term of accuracy as the different quantities are predicted differently by the model sets.

Additionally, the experimental case with the highest fluidization velocity could not be modeled with kinetic theory of granular flow model set due to persistent divergence problems, which were most likely caused by overpacking. It is difficult to estimate how much this is due to the solution routine of the solver, the implementation of the model set, the used simulation settings, and other user defined parameter. For other experimental cases the kinetic theory of granular flow model set was used without issues even with dense regions. Without further investigation, it cannot be concluded that the powder modulus model set would be more robust.

The original hypothesis of a simpler closure model being faster can be confirmed, but only by using a fixed time step size, and even then the differences in computational times were moderate with the differences decreasing when the mesh density is increasing. When using the adaptive time stepping, the total computational times were shorter than with the fixed time step size and the kinetic theory of granular flow model set simulations were moderately faster with coarser meshes and a few percent longer with the finest mesh. This was due to the better convergence and utilization of longer time step sizes for the kinetic theory of granular flow model set compared to the powder modulus model set. These results may vary in other geometries and simulation cases.

The results also indicate that the drag model, which often receives much attention in investigations, is not the only model to affect the particle distribution and velocities. Based on the results presented, the models governing the interaction of the particles also play an important role, especially in the prediction of the vertical pressure profile. It should be noted that the cases simulated here had densely packed regions where the significance of particle interactions are higher compared to dilute systems. It should be noted and as demonstrated here that while the vertical pressure is often used in verification of CFB modeling, alone it is not enough, as other macroscopic characteristics can be severely misestimated, such as the circulation rate of the particles, for example. Therefore, it is recommended to verify the modeling results with at least some other method.

In the future, more experimental measurement points are planned to be included to also obtain information higher in the riser, as measurement results were not available in the top parts of the riser. Additionally, the effect of the gas phase turbulence and the inclusion of the particle phase turbulence should be investigated.

Acknowledgement

The authors would like to acknowledge the financial support for this research from the Academy of Finland under Grant No. 278641.

Notation

Symbols

A	constant	[–]
C_D	drag coefficient	[–]
d	diameter	[m]
e	coefficient of restitution	[–]
$\mathbf{F}$	force	[N]
$\mathbf{g}$	gravitational acceleration	[m s^{-2}]
g_0	radial distribution function	[–]
I	second deviatoric stress tensor	[–]
K	momentum exchange coefficient	[kg m^{-3} s^{-1}]
k	solids thermal conductivity	[kg m^{-1} s^{-1}]
p	pressure	[Pa]
Re	Reynolds number	[–]
S	source term	[kg s^{-1} or Pa]
t	time	[s]
u	vector velocity	[–]
α	volume fraction	[–]
γ	dissipation of granular energy	[kg m^{-3} s^{-1}]
θ	granular temperature	[m^2 s^{-2}]
λ	bulk viscosity	[Pa s]
μ	dynamic viscosity	[kg s^{-1} m^{-1}]
ρ	density	[kg m^{-3}]
τ	shear stress	[Pa]
ϕ	angle of internal friction	[°]

Subscripts

col	collisional
fr	frictional
g	gas
kin	kinetic
max	maximum
rgh	hydrodynamic
s	solid
ss	solid-solid

References

Adamczyk, W.P., Klimanek, A., Białecki, R.A., Węcel, G., Kozołub, P., Czakiert, T., 2014a. Comparison of the standard Euler–Euler and hybrid Euler–Lagrange approaches for modeling particle transport in a pilot-scale circulating fluidized bed. Particuology 15, 129–137.

Adamczyk, W.P., Węcel, G., Klajny, M., Kozołub, P., Klimanek, A., Białecki, R.A., 2014b. Modeling of particle transport and combustion phenomena in a large-scale circulating fluidized bed boiler using a hybrid Euler–Lagrange approach. Particuology 16, 29–40.

Alves, J.J.N., Mori, M., 1998. Fluid dynamic modelling and simulation of circulating fluidized bed reactors: analyses of particle phase stress models. Comput. Chem. Eng. 22, S763–S766. https://doi.org/10.1016/S0098-1354(98)00143-4

Armstrong, L.M., Luo, K.H., Gu, S., 2010. Two-dimensional and three-dimensional computational studies of hydrodynamics in the transition from bubbling to circulating fluidised bed. Chem. Eng. J. 160, 239–248. https://doi.org/10.1016/j.cej.2010.02.032

Bona, L., Nan, Z., Wei, W., Jinghai, L., H., C.J., G., K.S., 2013. 3-D full-loop simulation of an industrial-scale circulating fluidized-bed boiler. AIChE J. 59, 1108–1117. https://doi.org/10.1002/aic.13917

Chan, C.W., Seville, J., Yang, Z., Baeyens, J., 2009. Particle motion in the CFB riser with special emphasis on PEPT-imaging of the bottom section. Powder Technol. 196, 318–325. https://doi.org/10.1016/j.powtec.2009.08.019

Chaouki, J., Larachi, F., Duduković, M.P., 1997. Noninvasive Tomographic and Velocimetric Monitoring of Multiphase Flows. Ind. Eng. Chem. Res. 36, 4476–4503. https://doi.org/10.1021/ie970210t

Cloete, S., Amini, S., Johansen, S.T., 2011. A fine resolution parametric study on the numerical simulation of gas–solid flows in a periodic riser section. Powder Technol. 205, 103–111. https://doi.org/10.1016/J.POWTEC.2010.08.072

Daikeler, A., Ströhle, J., Epple, B., 2017. Experimental investigation of the flow hydrodynamics in a 1 MWth dual fluidized bed pilot plant with a capacitance probe, in: 12th International Conference on Fluidized Bed Technology. Krakow, pp. 125–132.

de Velden, M. Van, Baeyens, J., Seville, J.P.K., Fan, X., 2008. The solids flow in the riser of a Circulating Fluidised Bed (CFB) viewed by Positron Emission Particle Tracking (PEPT). Powder Technol. 183, 290–296. https://doi.org/http://dx.doi.org/10.1016/j.powtec.2007.07.027

Dubrawski, K., Tebianian, S., Bi, H.T., Chaouki, J., Ellis, N., Gerspacher, R., Jafari, R., Kantzas, A., Lim, C., Patience, G.S., Pugsley, T., Qi, M.Z., Zhu, J.X., Grace, J.R., 2013. Traveling column for comparison of invasive and non-invasive fluidization voidage measurement techniques. Powder Technol. 235, 203–220. https://doi.org/10.1016/J.POWTEC.2012.10.031

Ellis, N., Bi, H.T., Lim, C.J., Grace, J.R., 2004. Hydrodynamics of turbulent fluidized beds of different diameters. Powder Technol. 141, 124–136. https://doi.org/10.1016/J.POWTEC.2004.03.001

Enwald, H., Peirano, E., Almstedt, A.-E., 1996. Eulerian two-phase flow theory applied to fluidization. Int. J. Multiph. Flow 22, Supple, 21–66. https://doi.org/http://dx.doi.org/10.1016/S0301-9322(96)90004-X

Ergun, S., 1952. Fluid flow through packed columns. Chem. Eng. Prog. 48, 89–94.

Farzaneh, M., Almstedt, A.-E., Johnsson, F., Pallarès, D., Sasic, S., 2015. The crucial role of frictional stress models for simulation of bubbling fluidized beds. Powder Technol. 270, 68–82. https://doi.org/10.1016/J.POWTEC.2014.09.050

Fox, R.O., 2014. On multiphase turbulence models for collisional fluid–particle flows. J. Fluid Mech. 742, 368-424.

Gidaspow, D., Bezburuah, R., Ding, J., 1991. Hydrodynamics of circulating fluidized beds: Kinetic theory approach., in: 7th International Conference on Fluidization, Gold Coast (Australia).

Jalali, P., Nikku, M., Hyppänen, T., 2013. Particle-cloud drag force in dilute particle systems: Discrete element method versus Eulerian simulations. Ind. Eng. Chem. Res. 52. https://doi.org/10.1021/ie302704j

Jin, B., Wang, X., Zhong, W., Tao, H., Ren, B., Xiao, R., 2010. Modeling on High-Flux Circulating Fluidized Bed with Geldart Group B Particles by Kinetic Theory of Granular Flow. Energy & Fuels 24, 3159–3172. https://doi.org/10.1021/ef100096c

Johnson, P.C., Nott, P., Jackson, R., 1990. Frictional–collisional equations of motion for participate flows and their application to chutes. J. Fluid Mech. 210, 501. https://doi.org/10.1017/S0022112090001380

Johnsson, H., Johnsson, F., 2001. Measurements of local solids volume-fraction in fluidized bed boilers. Powder Technol. 115, 13–26. https://doi.org/10.1016/S0032-5910(00)00270-9

Lu, G., Third, J.R., Müller, C.R., 2015. Discrete element models for non-spherical particle systems: From theoretical developments to applications. Chem. Eng. Sci. 127, 425–465. https://doi.org/http://dx.doi.org/10.1016/j.ces.2014.11.050

Lun, C.K.K., Savage, S.B., 1986. The effects of an impact velocity dependent coefficient of restitution on stresses developed by sheared granular materials. Acta Mech. 63, 15–44. https://doi.org/10.1007/BF01182538

Lun, C.K.K., Savage, S.B., Jeffrey, D.J., Chepurniy, N., 1984. Kinetic theories for granular flow: inelastic particles in couette flow and slightly inelastic particles in a general flow field. J. Fluid Mech. 140, 223–256.

Magnusson, A., Rundqvist, R., Almstedt, A.E., Johnsson, F., 2005. Dual fibre optical probe measurements of solids volume fraction in a circulating fluidized bed. Powder Technol. 151, 19–26. https://doi.org/10.1016/J.POWTEC.2004.11.028

Malcus, S., Chaplin, G., Pugsley, T., 2000. The hydrodynamics of the high-density bottom zone in a CFB riser analyzed by means of electrical capacitance tomography (ECT). Chem. Eng. Sci. 55, 4129–4138. https://doi.org/10.1016/S0009-2509(00)00083-X

Massoudi, M., Rajagopal, K.R., Ekmann, J.M., Mathur, M.P., 1992. Remarks on the modeling of fluidized systems. AIChE J. 38, 471–472. https://doi.org/10.1002/aic.690380317

Maurer, S., Wagner, E.C., van Ommen, J.R., Schildhauer, T.J., Teske, S.L., Biollaz, S.M.A., Wokaun, A., Mudde, R.F., 2015. Influence of vertical internals on a bubbling fluidized bed characterized by X-ray tomography. Int. J. Multiph. Flow 75, 237–249. https://doi.org/10.1016/J.IJMULTIPHASEFLOW.2015.06.001

Nikku, M., Jalali, P., Hyppänen, T., 2017. Comparison of Ansys Fluent and OpenFOAM is simulation of circulating fluidized bed riser, in: Nowak, W., Marek, S., Pawel, M. (Eds.), Proceedings of the 12th International Conference of Fluidized Bed Technology. Krakow, pp. 349–356.

Nikku, M., Myöhänen, K., Ritvanen, J., Hyppänen, T., Lyytikäinen, M., 2016. Three-dimensional modeling of biomass fuel flow in a circulating fluidized bed furnace with an experimentally derived momentum exchange model. Chem. Eng. Res. Des. 115. https://doi.org/10.1016/j.cherd.2016.09.023

Nikolopoulos, A., Stroh, A., Zeneli, M., Alobaid, F., Nikolopoulos, N., Ströhle, J., Karellas, S., Epple, B., Grammelis, P., 2017. Numerical investigation and comparison of coarse grain CFD – DEM

and TFM in the case of a 1 MWth fluidized bed carbonator simulation. Chem. Eng. Sci. 163, 189–205. https://doi.org/10.1016/J.CES.2017.01.052

Panday, R., Shadle, L.J., Shahnam, M., Cocco, R., Issangya, A., Spenik, J.S., Ludlow, J.C., Gopalan, B., Shaffer, F., Syamlal, M., Guenther, C., Karri, S.B.R., Knowlton, T., 2014. Challenge problem: 1. Model validation of circulating fluidized beds. Powder Technol. 258, 370–391. https://doi.org/10.1016/j.powtec.2014.02.010

Passalacqua, A., Marmo, L., 2009. A critical comparison of frictional stress models applied to the simulation of bubbling fluidized beds. Chem. Eng. Sci. 64, 2795–2806. https://doi.org/10.1016/J.CES.2009.03.005

Patil, D.J., van Sint Annaland, M., Kuipers, J.A.M., 2005a. Critical comparison of hydrodynamic models for gas–solid fluidized beds—Part I : bubbling gas–solid fluidized beds operated with a jet. Chem. Eng. Sci. 60, 57–72. https://doi.org/10.1016/J.CES.2004.07.059

Patil, D.J., van Sint Annaland, M., Kuipers, J.A.M., 2005b. Critical comparison of hydrodynamic models for gas–solid fluidized beds—Part II: freely bubbling gas–solid fluidized beds. Chem. Eng. Sci. 60, 73–84. https://doi.org/10.1016/J.CES.2004.07.058

Peltola, J., 2009. Dynamics in a circulating fluidzed bed: Experimental and numerical study. Tampere University of Technology.

Pugsley, T., Tanfara, H., Malcus, S., Cui, H., Chaouki, J., Winters, C., 2003. Verification of fluidized bed electrical capacitance tomography measurements with a fibre optic probe. Chem. Eng. Sci. 58, 3923–3934. https://doi.org/10.1016/S0009-2509(03)00288-4

Qiu, X., Wang, L., Yang, N., Li, J., 2017. A simplified two-fluid model coupled with EMMS drag for gas-solid flows. Powder Technol. 314, 299–314. https://doi.org/10.1016/J.POWTEC.2016.09.002

Savage, S.B., 1988. Streaming motions in a bed of vibrationally fluidized dry granular material. J. Fluid Mech. 194, 457. https://doi.org/10.1017/S0022112088003064

Schaeffer, D.G., 1987. Instability in the evolution equations describing incompressible granular flow. J. Differ. Equ. 66, 19–50.

Shah, M.T., Utikar, R.P., Pareek, V.K., Evans, G.M., Joshi, J.B., 2016. Computational fluid dynamic modelling of FCC riser: A review. Chem. Eng. Res. Des. 111, 403–448. https://doi.org/10.1016/j.cherd.2016.04.017

Shah, S., Myöhänen, K., Kallio, S., Hyppänen, T., 2015a. CFD simulations of gas–solid flow in an industrial-scale circulating fluidized bed furnace using subgrid-scale drag models. Particuology 18, 66–75. https://doi.org/http://dx.doi.org/10.1016/j.partic.2014.05.008

Shah, S., Myöhänen, K., Kallio, S., Ritvanen, J., Hyppänen, T., 2015b. CFD modeling of gas-solids flow in a large scale circulating fluidized bed furnace. Powder Technol. 274, 239–249. https://doi.org/10.1016/j.powtec.2015.01.019

Sinclair, J.L., Jackson, R., 1989. Gas-particle flow in a vertical pipe with particle-particle interactions. AIChE J. 35, 1473–1486.

Syamlal, M., Rogers, W., O`Brien, T.J., 1993. MFIX documentation theory guide 1004. https://doi.org/10.2172/10145548

Tortora, P.R., Ceccio, S.L., Mychkovsky, A.G., O'Hern, T.J., Torczynski, J.R., 2008. Radial profiles of solids loading and flux in a gas–solid circulating fluidized bed. Powder Technol. 180, 312–320. https://doi.org/10.1016/J.POWTEC.2007.09.007

van Wachem, B.G.M., Schouten, J.C., van den Bleek, C.M., Krishna, R., Sinclair, J.L., 2001. Comparative analysis of CFD models of dense gas-solid systems. AIChE J. 47, 1035–1051.

https://doi.org/10.1002/aic.690470510

Weber, J.M., Bobek, M.M., Breault, R.W., Mei, J.S., Shadle, L.J., 2018. Investigation of core-annular flow in an industrial scale circulating fluidized bed riser with electrical capacitance volume tomography (ECVT). Powder Technol. 327, 524–535. https://doi.org/10.1016/J.POWTEC.2017.12.094

Wen, C.Y., Yu, Y.H., 1966. Mechanics of fluidization. Chem. Eng. Prog. Symp. Ser. 62, 100–111.

Wiesendorf, V., Werther, J., 2000. Capacitance probes for solids volume concentration and velocity measurements in industrial fluidized bed reactors. Powder Technol. 110, 143–157. https://doi.org/10.1016/S0032-5910(99)00276-4

Yang, D., Liu, L., Feng, W., 2018. Experimental investigation of an internally circulating fluidized bed with 32-electrode Electrical Capacitance Volume Tomography. Measurement. https://doi.org/10.1016/j.measurement.2018.05.076

Ye, S., Qi, X., Zhu, J., 2009. Direct measurements of instantaneous solid flux in a circulating fluidized bed riser using a novel multifunctional optical fiber probe. Chem. Eng. Technol. 32, 580–589. https://doi.org/10.1002/ceat.200800361

Zhao, Y., Ding, T., Zhu, L., Zhong, Y., 2016. A Specularity Coefficient Model and Its Application to Dense Particulate Flow Simulations. Ind. Eng. Chem. Res. 55, 1439–1448. https://doi.org/10.1021/acs.iecr.5b03792

Zhao, Y., Lu, B., Zhong, Y., 2015. Influence of collisional parameters for rough particles on simulation of a gas-fluidized bed using a two-fluid model. Int. J. Multiph. Flow 71, 1–13. https://doi.org/10.1016/J.IJMULTIPHASEFLOW.2014.12.002

Zheng, Y., Wan, X., Qian, Z., Wei, F., Jin, Y., 2001. Numerical simulation of the gas–particle turbulent flow in riser reactor based on k–ε–kp–εp–Θ two-fluid model. Chem. Eng. Sci. 56, 6813–6822. https://doi.org/10.1016/S0009-2509(01)00319-0

Zhou, X., Gao, J., Xu, C., Lan, X., 2013. Effect of wall boundary condition on CFD simulation of CFB risers. Particuology 11, 556–565. https://doi.org/10.1016/J.PARTIC.2012.08.006